coatings

MDPI

Article

Analysis of Surface Roughness and Flank Wear Using the Taguchi Method in Milling of NiTi Shape Memory Alloy with Uncoated Tools

Emre Altas [1,*], Hasan Gokkaya [2], Meltem Altin Karatas [3] and Dervis Ozkan [1]

1 Mechanical Engineering Department, Bartın University, Bartın 74100, Turkey; dervisozkan@bartin.edu.tr
2 Mechanical Engineering Department, Engineering Faculty, Karabuk University, Karabuk 78050, Turkey; hgokkaya@karabuk.edu.tr
3 Machinery and Metal Technology Department, Gerede Vocational School, Bolu Abant Izzet Baysal University, Bolu 14900, Turkey; meltemaltin@ibu.edu.tr
* Correspondence: emrealtas@bartin.edu.tr; Tel.: +90-378-5011-000

Received: 26 November 2020; Accepted: 16 December 2020; Published: 19 December 2020

Abstract: The aim of this study was to optimize machining parameters to obtain the smallest average surface roughness (Ra) and flank wear (Vb) values as a result of the surface milling of a nickel-titanium (NiTi) shape memory alloy (SMA) with uncoated cutting tools with different nose radius (r_ε) under dry cutting conditions. Tungsten carbide cutting tools with different r_ε (0.4 mm and 0.8 mm) were used in milling operations. The milling process was performed as lateral/surface cutting at three different cutting speeds (V_c) (20, 35 and 50 m/min), feed rates (f_z) (0.03, 0.07 and 0.14 mm/tooth) and a constant axial cutting depth (0.7 mm). The effects of machining parameters in milling experiments were investigated based on the Taguchi L18 ($2^1 \times 3^2$) orthogonal sequence, and the data obtained were analyzed using the Minitab 17 software. To determine the effects of processing parameters on Ra and Vb, analysis of variance (ANOVA) was used. The analysis results reveal that the dominant factor affecting the Ra is the cutting tool r_ε, while the main factor affecting Vb is the f_z. Since the predicted values and measured values are very close to each other, it can be said that optimization is correct according to the validation test results.

Keywords: NiTi shape memory alloy; average surface roughness; flank wear; milling; Taguchi optimization

1. Introduction

In our daily life, the demand for functional products due to the problems encountered in medicine and industrial areas has led scientists to improve the properties of materials and to produce new materials with superior properties. Smart materials, which have made great progress in recent years, have the ability to change their properties according to environmental conditions. Smart materials are used to transform one type of energy into other [1]. The use of smart materials is increasing in the biomedical, aerospace, and automotive industries. Shape memory alloys (SMAs), which are among smart materials, can return to their original form (shape or size) when subjected to a recall process between two transformation phases dependent on temperature or magnetic field [2].

Among the SMAs, nickel-titanium (NiTi) alloy is the most widely used one in the biomedical field. The most important difference of the NiTi SMA from other engineering materials is that it undergoes a phase change when exposed to heat or load, which causes the material to have shape memory and return to its original shape with increasing temperature [3]. At low temperatures, the NiTi alloy is in the martensitic phase, while it is in the austenitic phase at high temperatures [4].

When the literature is examined, it is seen that unconventional manufacturing methods such as the laser processing method [5], electro discharge machining (EDM) [6], electrochemical polishing [7] and abrasive water jet method (AWJM) [8] are used to shape NiTi alloy, along with traditional machining methods of turning [9], milling [10] and drilling [11]. The NiTi components produced by laser cutting or EDM have a straight profile on the surface. Electropolishing is used to reduce the surface roughness of these components. However, the milling process is used to obtain complexly shaped and large parts consisting of NiTi alloys. Micro-milling is a good method in the machining of small-scaled parts; however, as far as large parts are concerned, conventional milling is a more appropriate method due to its higher productivity and lower cost. For a machining processes like milling, NiTi SMAs are known as hard to machine materials, mainly due to their shape memory and super-elasticity effects, their high ductility, and deformation hardening, which lead to poor surface finish and poor tool life [9]. High ductility is responsible for the sticking of chips on the cutting edge and burr formation on the edges of machined surface. Deformation hardening causes high cutting forces and temperatures. The hardness of conventional materials decreases with cutting temperature, which provides lower cutting forces. However, in the case of NiTi SMA, the material may have a phase transformation with the effect of mechanical and thermal loads. The alloy in the present study is in the austenite phase at room temperature. When a load is applied onto the alloy, the austenite transforms into a martensite structure. As deformation hardening ability of the martensite phase is higher than that of austenite, it causes higher cutting forces and temperatures [12]. In addition, the changing elastic modulus of the alloy during the cutting process causes a decrease in the machinability and dimensional precision of the alloy [12,13]. Therefore, researchers investigated the ways of machining with lower surface roughness, lower tool wear, lower chip formation and of saving surface integrity of the material during the cutting process.

In the literature, Wang et al. carried out milling experiments using a titanium aluminum nitride/titanium nitride (TiAlN/TiN)-coated carbide end mill to investigate the effect of cutting parameters on the work hardening of $Ni_{50.8}Ti_{49.2}$ SMA. As a result of the experimental studies, the researchers determined that the most important parameter affecting the work hardening was the cutting speed (V_c). When the effect of the feed rate (f_z) on the work hardening was examined, they observed that work hardening increased with the increase in the f_z [14]. Guo et al. analyzed the surface integrity of the alloy due to tool wear, burr formation, and the formation of a white layer on the workpiece surface during the processing of NiTi SMA by milling and the electro discharge machining (EDM) method. The wear on the face of the tool in contact with the machined surface of the alloy is called flank wear. The wear in the shape of a notch on the cutting edge is called notch wear. After the milling experiments were conducted using TiAlN/TiN-coated tungsten carbide cutting tools, the researchers stated that flank wear, coating rupture, notch wear and micro notching are the types of wear on cutting tools [15]. Kuppuswamy and Yui conducted a study on the main cutting forces and optimization of machining parameters in order to minimize burr formation in the milling of NiTi alloy. They determined the order of importance of cutting parameters to reduce cutting forces and burr size as cutting speed (V_c), feed rate (f_z), and cutting depth, respectively [10]. Weinert and Petzoldt examined tool wear and machining quality in micro-milling processes of NiTi SMA. After their cutting tests, they achieved the best machining quality at 10 µm cutting depth. They observed that high cutting width and high f_z provide better chip formation and increase tool life and workpiece quality. However, they stated that they could not completely prevent burr formation [9].

Kaya and Kaya investigated the wear behavior of polycrystalline diamond (PCD) and polycrystalline cubic boron nitride (PCBN) cutting tools used in the turning process of NiTi shape memory alloy. Researchers stated that PCD tools showed better wear resistance in all cutting speeds of machining tests [3].

Our literature review revealed that no studies have yet been conducted on the processing of NiTi SMA with cutting tools with different nose radii (r_ε) on a milling machine. Nose radius is an important feature of cutting tools which affects the surface quality of machined materials. A larger nose radius

makes the tool stronger and surface finish better, while it leads to higher cutting forces. Increasing cutting forces causes higher tool wear, vibrations, and poor surface finish. Therefore, a good decision has to be made regarding nose radius depending on the type of workpiece material. The studies in the literature are mostly micro-milling studies conducted with carbide end mills. However, the conventional milling process has a huge potential to be used in the production of large-sized plates used for joining bones in the medical sector and some future parts in the automotive sector such as engine cooling, carburetor and engine lubrication controls, and the control of a radiator blind [16]. In this study, the surface milling of NiTi SMA was investigated under dry cutting conditions, with cutting tools with different r_ε, and using different machining parameters. Following the machining process, the effects of machining parameters on flank wear and workpiece surface quality were optimized and investigated. In order to minimize the effect of coating layer in the determination of the effect of other machining parameters, uncoated tools were used in the cutting tests. Thus, we aimed to provide reference information to select optimal cutting parameters for further studies on coating application on carbide cutting tools. Low surface roughness and low tool wear are desired in all these products for sustainable manufacturing with high productivity and low cost. Therefore, it is highly important to determine optimum machining parameters in terms of both productivity and effective service of the product. The study clearly presents the optimum cutting parameters to be used in the milling of NiTi SMAs with carbide tools.

2. Materials and Methodology

2.1. Workpiece Material

In the experimental studies, NiTi SMA, which is used for joining broken bones in orthopedics, was used as the workpiece. The NiTi SMA used in the study was produced with the vacuum arc remelting (VAR) method and then subjected to hot rolling. The starting surface roughness of the alloy was an average surface roughness (Ra) of 0.31 µm. It was in the austenite phase at room temperature, contained 55.8% of Ni element (% Weight) in its structure, and had a size of 25 × 100 × 100 mm. Two pieces of the workpiece were used in cutting tests. Table 1 presents the chemical composition of the NiTi SMA determined by an X-ray diffractometer (Smartlab, Rigaku, Tokyo, Japan). Mechanical properties of the alloy were measured with tensile test equipment (Shimadzu AG-X) according to ASTM E8 and the results are given in Table 2. The stress–strain curve of the alloy obtained through the tensile test carried out at room temperature is shown in Figure 1. The superelastic effect on unloading is seen in the dotted line.

Table 1. The chemical composition of the nickel-titanium (NiTi) shape memory alloy (SMA) (% Weight).

Ni	C	Co	Cu	Cr	H	Fe	Nb	N+O	Ti
55.8	0.038	0.005	0.006	0.004	0.001	0.0012	0.005	0.041	44.09

Table 2. The mechanical properties of the NiTi SMA.

Yield Strength, (MPa)	Tensile Strength, (MPa)	% Elongation	Hardness, (HRC)
280	630	13.9	26.5

The phase transformation temperatures of the alloy were measured using the diffraction scanning calorimetry (DSC) method according to ASTM D3418 under temperatures of 20–25 °C and a humidity of 50%–70%, and the applied processes are given in Table 3. Figure 2 also represents the phase transformation–temperature graph of the alloy. Phase transformation temperatures of martensite start (M_s), martensite finish (M_f), austenite start (A_s), and austenite finish (A_f) were measured as −10.95, −49.87, −32.99 and 8.79 °C, respectively. The temperature values in Table 3 show that NiTi alloy was in the austenite phase at room temperature before processing. R-phase was not observed in the alloy.

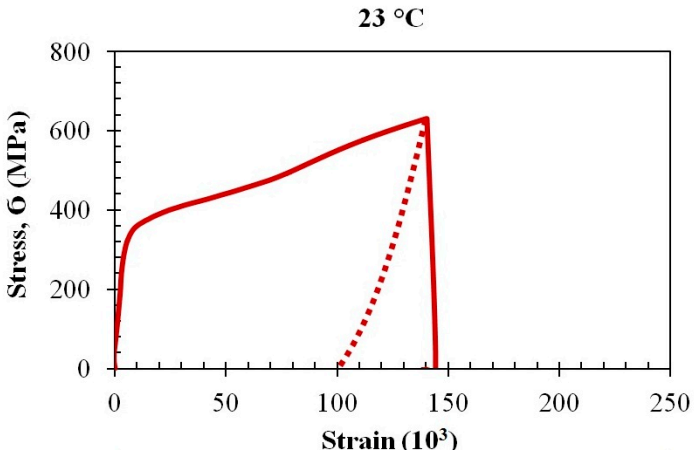

Figure 1. Stress–strain curve of NiTi SMA.

Table 3. Phase transformation temperatures of the NiTi SMA.

Melting Method	Treatment	M_f (°C)	M_s (°C)	A_s (°C)	A_f (°C)
Vacuum Arc Method	Hot Rolling	−49.87	−10.95	−32.99	8.79

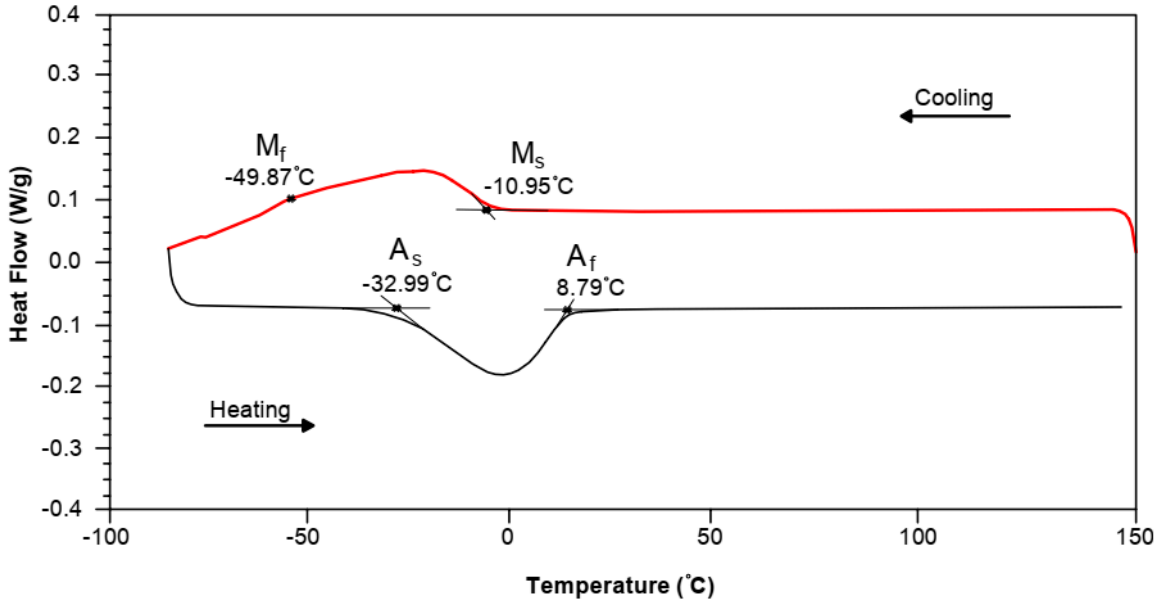

Figure 2. Phase transformation-temperature graph of NiTi SMA.

2.2. Cutting Tools

In the machining of NiTi SMAs with the milling machine, uncoated tungsten carbide cutting tools produced by the Sandvik Coromant company were used. One was the R39011T308E (NLH13A) with r_ε = 0.8 mm and the other was the R39011T304E (NLH13A) with r_ε = 0.4 mm. In order to create the same conditions in all of the experiments, new cutting tools that had never been used previously were used in each experiment. After each experiment, the machine was stopped, and the V_c and f_z were changed. A total of 18 experiments were performed, with 9 tests for each type of cutting tool with different r_ε. The geometric dimensions of the cutting tools selected in accordance with ISO 1832:2017 are given in Figure 3.

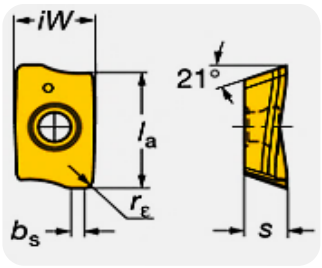

	l_a	iW	S	b_s	r_ε
Dimensions [mm]	10	6.8	3.5	0.9	0.4
	10	6.8	3.5	1.2	0.8

Figure 3. The geometric dimensions of the cutting tools used in milling operation.

In the experiments, R390-025A25-11L double-edged tool holder suitable for replaceable tips was used. The tool holder was selected with reference to ISO 5608 [17]. The experiments were carried out by mounting a cutting tool on the tool holder in order to provide fixed machining parameters.

2.3. Cutting Tests

For the machining process, an industrial CNC milling machine "Falco VMC 855-B" with a power of 7.5 kW was used. The general view of the milling process is shown in Figure 4.

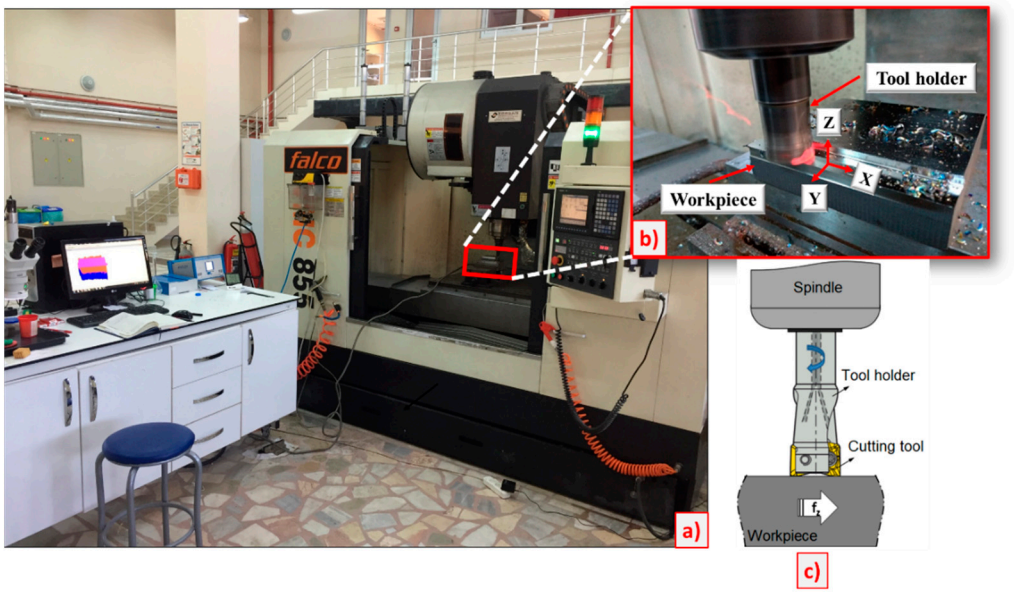

Figure 4. The symbolic representation of (**a**) the milling machine, (**b**) the experimental setup, and (**c**) the face milling process used in cutting tests.

In the experiments, the amount of cutting tool wear and the Ra of the workpiece were measured at the end of each 100 mm cutting length during the cutting process. The measurement of workpiece Ra values was performed after each cutting depth was removed from the surface. Following each experiment, the cutting process was paused, and the tool wear depth measurement was performed with an stereo zoom microscope (Vision SX45, New York, NY, USA). The types of wear were categorized as flank wear, built-up edge (BUE), mechanical fatigue fracture, fracture wear and crater wear in order of effect and prevalence. BUE is a wear type that forms as the chip sticks on the top (rake) surface of the cutting tool. Wear in a crater shape that occurs on the rake surface of cutting tool due to the friction between chip and tool is called crater wear. Flank wear depth (Vb) due to the abrasive wear

mechanism was taken into account while comparing the amount of wear and determining tool life. During the cutting tests, a CCD camera mounted on the stereo zoom microscope was utilized in order to measure the amount of flank wear (Vb) that occurs on the cutting tools. In the surface milling process, the free surface wear amount of the cutting tool was taken as 0.3 mm according to the TS ISO-8688 standard. To measure Ra, the Surftest SJ-310 tipped Ra device (Mitutoyo, Germany) was used (Figure 5). After each cutting process, roughness values taken from three different points from the machined workpiece surface were recorded. Ra values were determined by taking the arithmetic mean of three different values. The wear mechanism on the cutting tools was investigated with the FEI Quanta FEG 250 type scanning electron microscope (SEM, ThermoFisher Scientific, Waltham, MA, USA) and an energy dispersive spectroscope (EDS, ThermoFisher Scientific).

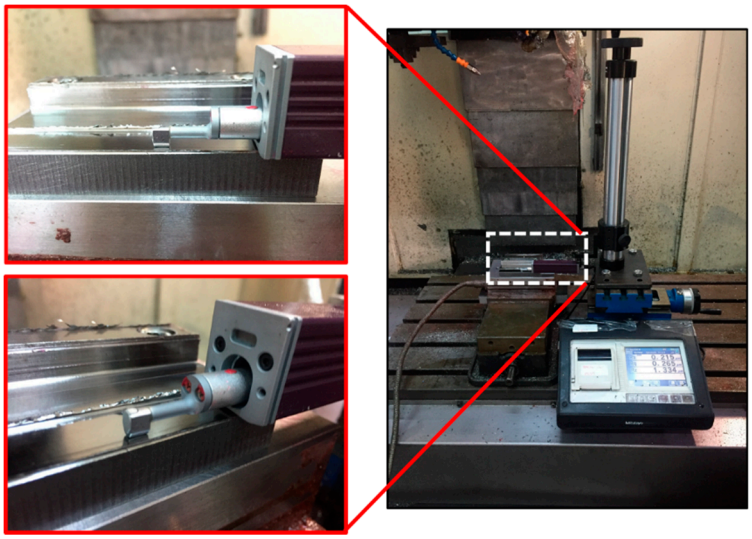

Figure 5. Image of Ra measurement moment.

2.4. Experimental Design and the Taguchi Method

Taguchi experimental design method is a scientific and effective method that helps a designer to determine near-optimum settings of the design parameters of the experimental process. This analysis is performed using the signal-to-noise (S/N) ratio [18]. There are three different quality values here: "nominal is best", "smaller is better" and "larger is better". In this study, the minimum value was taken for the best Ra and Vb, and "smaller is better" was selected to calculate the optimal S/N ratio for the minimum Ra and Vb. The S/N ratio calculation was determined as "smaller is better", given in Equation (1) [19].

$$\frac{S}{N} = -10 \log\left[\frac{1}{n}\sum_{i=1}^{n} {y_i}^2\right] \quad (1)$$

In Equation (1), "n" is the number of tests and "y_i" is the observed data in the experiment.

3. Results and Discussion

3.1. Experimental Results and Taguchi Optimization for Ra and Vb

In this study, a tungsten carbide cutting tool with two different r_ε, three different V_c and three different f_z were selected as the processing parameters whose effects will be analyzed, and the milling experiments were carried out at the levels given in Table 4. The axial depth of the cut (a_p = 0.7 mm) and radial depth of the cut (a_e = 15 mm) were kept constant. In order to specify the optimum cutting parameters and to analyze the impacts of the specified cutting parameters on Ra and Vb, the Taguchi method was used and L18 ($2^1 \times 3^2$) (mixed orthogonal array) was selected (Table 5). Among the

control factors specified in the table, "A" indicates the r_ε of cutting tool, "B" indicates the V_c, and "C" indicates the f_z.

Table 4. Cutting tool and machining parameters used in the milling process.

Symbol	Parameters	Units	Level 1	Level 2	Level 3
r_ε	Nose radius of tungsten carbide cutting tools	(mm)	0.4	0.8	–
V_c	Cutting speed	(m/min)	20	35	50
f_z	Feed rate	(mm/tooth)	0.03	0.07	0.14

Table 5. The experimental design L_{18} ($2^1 \times 3^2$).

Test Nr.	A (r_ε)	B (V_c)	C (f_z)
1	1	1	1
2	1	1	2
3	1	1	3
4	1	2	1
5	1	2	2
6	1	2	3
7	1	3	1
8	1	3	2
9	1	3	3
10	2	1	1
11	2	1	2
12	2	1	3
13	2	2	1
14	2	2	2
15	2	2	3
16	2	3	1
17	2	3	2
18	2	3	3

In the experimental study, three different V_c (20, 35 and 50 m/min) and three different f_z (0.03, 0.07 and 0.14 mm/tooth) were used, and NiTi SMA was milled in dry conditions using uncoated tungsten carbide cutting tools with two different r_ε (0.4 and 0.8 mm). In the Taguchi method, S/N ratios are used to evaluate the variations in design of experiment. According to this method, in order to perform statistical analysis, the Ra values were converted into the S/N ratio based on the "smaller is the better" approach (Table 6). While the signal value represents the actual value given by the system that needs to be measured, the noise factor represents the rate of unwanted factors in the measured value [20]. In the experimental study, the Ra value was measured as 0.543 µm, and the average S/N ratio for the Ra value was obtained as 5.503 dB. The average Vb value was measured as 0.621 mm and the average S/N ratio for the Vb value was obtained as 4.790 dB.

In addition, the impact of each control factor (A, B and C) on Ra and Vb was analyzed using the S/N ratio response table (Table 7). The determined levels of control factors for Ra and Vb are shown in Table 7. The impacts of control factors and levels on Ra and Vb are given in Figure 6. The optimum level for both Ra and Vb values was obtained as A2B1C1.

Table 6. The signal-to-noise (S/N) ratios for Ra and Vb.

	Machining Parameters and Their Levels						
	A	**B**	**C**				
Test Nr.	**Nose Radius of Tools, r_ε**	**Cutting Speed, V_c**	**Feed Rate, f_z**	**Measured Average Surface Roughness, Ra (μm)**	**Calculated S/N Ratio (n_i = 1–18)**	**Measured Flank Wear, Vb**	**Calculated S/N Ratio (n_i = 1–18)**
	(mm)	**(m/min)**	**(mm/tooth)**		**(dB)**	**(mm)**	**(dB)**
1	0.4	20	0.03	0.424	7.453	0.435	7.230
2	0.4	20	0.07	0.522	5.647	0.642	3.849
3	0.4	20	0.14	0.645	3.809	0.804	1.895
4	0.4	35	0.03	0.612	4.265	0.668	3.505
5	0.4	35	0.07	0.678	3.375	0.856	1.351
6	0.4	35	0.14	0.692	3.198	0.915	0.772
7	0.4	50	0.03	0.546	5.256	0.650	3.742
8	0.4	50	0.07	0.615	4.222	0.683	3.312
9	0.4	50	0.14	0.736	2.662	0.942	0.519
10	0.8	20	0.03	0.346	9.218	0.264	11.568
11	0.8	20	0.07	0.381	8.382	0.281	11.026
12	0.8	20	0.14	0.538	5.384	0.701	3.086
13	0.8	35	0.03	0.519	5.697	0.353	9.045
14	0.8	35	0.07	0.554	5.130	0.704	3.049
15	0.8	35	0.14	0.572	4.852	0.736	2.662
16	0.8	50	0.03	0.384	8.313	0.284	10.934
17	0.8	50	0.07	0.420	7.535	0.463	6.688
18	0.8	50	0.14	0.585	4.657	0.796	1.982

Table 7. Response table of S/N ratios and mean values.

	Average Surface Roughness (Ra)			**Flank Wear Vb (mm)**		
Level	**A**	**B**	**C**	**A**	**B**	**C**
S/N Ratio						
1	4.432	6.649	6.700	2.908	6.442	7.670
2	6.574	4.419	5.715	6.671	3.397	4.879
3	-	5.441	4.094	-	4.529	1.819
Delta	2.142	2.229	2.607	3.763	3.045	5.851
Rank	3	2	1	2	3	1
Means						
1	0.6078	0.4760	0.4718	0.7328	0.5212	0.4423
2	0.4777	0.6045	0.5283	0.5091	0.7053	0.6048
3	-	0.5477	0.6280	-	0.6363	0.8157
Delta	0.1301	0.1285	0.1562	0.2237	0.1842	0.3733
Rank	2	3	1	2	3	1

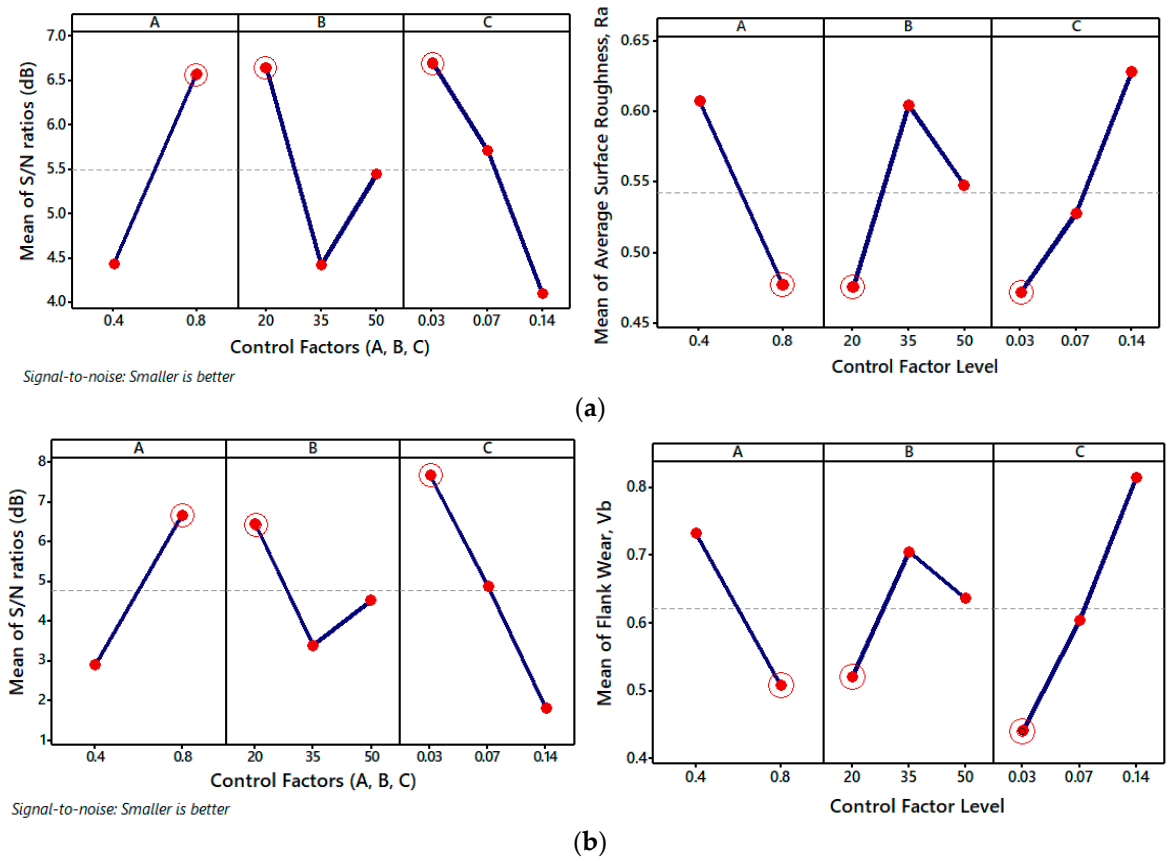

Figure 6. (**a**) Effect of control factors on Ra (**b**) Effect of control factors on Vb.

3.2. Effects of Cutting Parameters on Average Surface Roughness

The workpiece Ra values obtained by machining NiTi SMAs with tungsten carbide tools with two different r_ε (0.4 and 0.8 mm) at three different V_c and f_z are given in Figure 6a, in a control factors graph. When the Ra values obtained from the test results are examined, it is seen that the highest Ra (0.736 µm) was obtained at 50 m/min V_c and 0.14 mm/tooth f_z with the cutting tool with 0.4 mm r_ε, and the lowest Ra (0.346 µm) was obtained at 20 m/min V_c and 0.03 mm/tooth f_z with the cutting tool with 0.8 mm r_ε. When the Ra values obtained depending on the V_c are examined (Figure 6a), it is seen that the reason for obtaining low Ra at low V_c (20 m/min) is attributed to the (built-up edge (BUE) that formed on the cutting tool. The scanning electron microscope (SEM) image of the BUE formed on the cutting tool at 20 m/min V_c is shown in Figure 7a. The BUE forming on the cutting tool increases the cutting tool r_ε and contributes positively to the Ra value [14,21,22]. Increasing the V_c from 20 to 35 m/min increased the V_c and the Ra. This was attributed to the V_b (Figure 7b) on the cutting tool caused by high temperatures due to the friction coefficient at increasing V_c [3,23]. A 4% decrease (0.632 µm) was observed in the Ra with a 30% increase (50 m/min) in V_c at 35 m/min V_c. The Ra that improves with the increase in V_c can be explained by obtaining less deformation hardening due to the increasing temperature at high V_c, the easy deformation of the workpiece material around the cutting edge and r_ε, and the flow zone that emerges at these high temperatures [24,25]. The improvement in Ra due to the increase in V_c is an expected feature. Increasing V_c to improve Ra is consistent with the literature [26,27].

When the Ra obtained depending on the f_z is examined, it can be stated that the increase in Ra due to the increase in the f_z of both cutting tools is an expected feature in theory (Equation (2)), and the f_z should be reduced in order to reduce Ra [26]. High Ra at high f_z (0.14 mm/tooth) stems from cutting tool wear (Figure 7c). The findings obtained were similar to those in the literature [3,27].

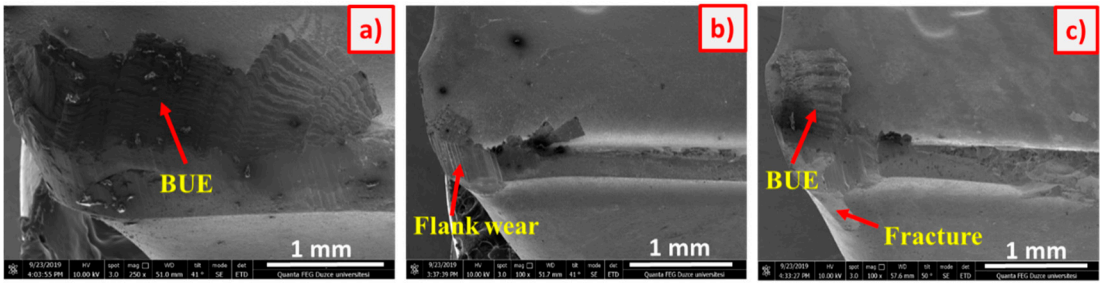

Figure 7. SEM image of built-up edge (BUE) (**a**), flank wear (**b**), and tool wear (**c**) that occurred on the cutting tool as a result of the milling of NiTi SMA under different machining parameters with the nose radius of 0.8 mm and at high feed rate (0.14 mm/tooth).

$$R_a = \frac{0.321 x f^2}{r_\varepsilon} \quad (2)$$

The surface graph in Figure 8 shows the effect of the cutting parameters on the Ra obtained as a result of the experimental study. When the graph is analyzed, it is seen that the Ra values increased with the increase in the f_z. This finding corroborates the evaluation performed based on the S/N ratios and is parallel to the theoretical formula (Equation (2)), which indicates that the Ra will increase in proportion to the square of the f_z. It is known that with the increase in the f_z, the temperature in the cutting zone increases [3,28], and the resulting heat is concentrated at the tool-chip and tool workpiece interface due to the low thermal conductivity of the NiTi SMA [26,27]. In this context, the increase in Ra values is an expected result, as permanent stress will increase on the processed surface with the increase in the f_z. On the other hand, it seems that the Ra tends to decrease with increasing r_ε. This result can be explained by chip formation due to decreased uncut chip thickness with increasing r_ε. It has been emphasized that the thickness of uncut chips along the cutting edge will decrease depending on the increase in the r_ε of the cutting tool [3,27]. With the decrease in chip thickness, a decrease is observed in cutting power and consequently cutting tool vibration [21].

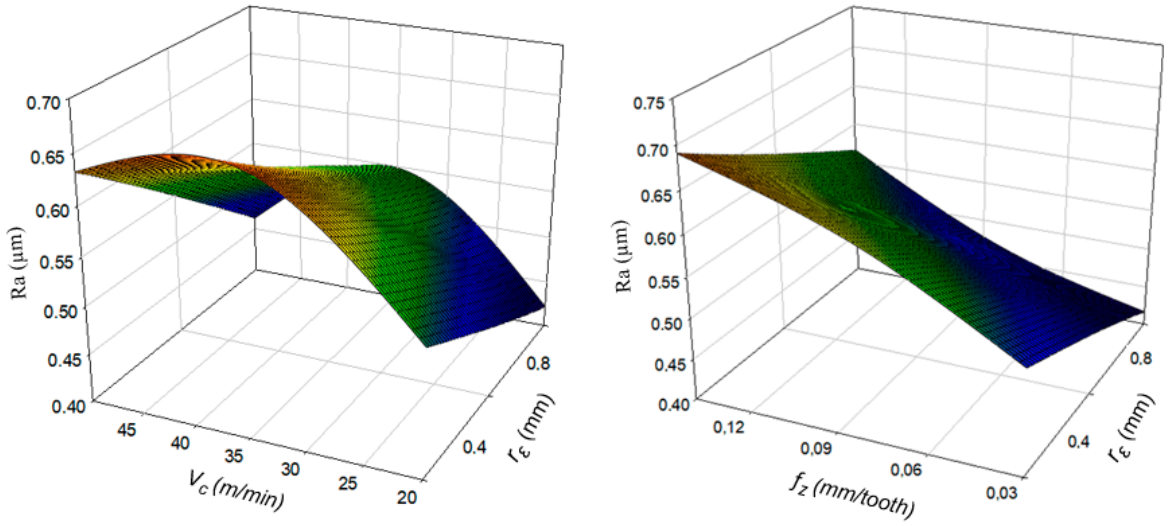

Figure 8. Effect of the cutting parameters on Ra.

3.3. *Effects of Cutting Parameters on Flank Wear*

As a result of the experimental study, it was determined that the high deformation hardening of the NiTi SMA causes abrasive wear, while its ductility causes adhesive wear. The Vb values obtained by machining NiTi SMAs with tungsten carbide tools with two different r_ε (0.4 mm and 0.8 mm) at

three different V_c and f_z are given in Figure 6b in a control factors graph. When the Vb values obtained from the experiments are examined, it is seen that the highest Vb occurred with the cutting tool with a 0.4 mm r_ε, at 50 m/min V_c and 0.14 mm/tooth f_z (0.942 mm). The lowest Vb occurred with the cutting tool with a 0.8 mm r_ε, at 20 m/min V_c and 0.03 mm/tooth f_z (0.264 mm). The tool life (0.942 mm) was completed at high V_c (50 m/min) and f_z (0.14 mm/tooth) (Figure 9a). The low Vb value at low V_c (20 m/min) and f_z (0.03 mm/tooth) was attributed to the formation of a BUE on the cutting tool (Figure 9b), which can be explained by the low temperature that occurs at the tool-chip interface [27,29]. Increasing temperature at the tool–chip interface at high V_c (50, m/min) also causes thermal softening in the cutting tool. Since the softening occurring in the workpiece at high V_c (50, m/min) is more than the thermal softening in the cutting tool, a decrease was observed in the Vb value of the cutting tool [3,27]. As seen in the graph in Figure 6b, the increase in the V_c and f_z at three different V_c (20, 35 and 50 m/min) and f_z (0.03, 0.07 and 0.14 mm/tooth) depends on the increase in the cutting temperature between the cutting tool and the workpiece. It is thought that the chemical reaction occurring between the carbide cutting tool and the workpiece with the influence of increasing temperature affects the wear on the cutting tool and increases Vb formation [3,26,27].

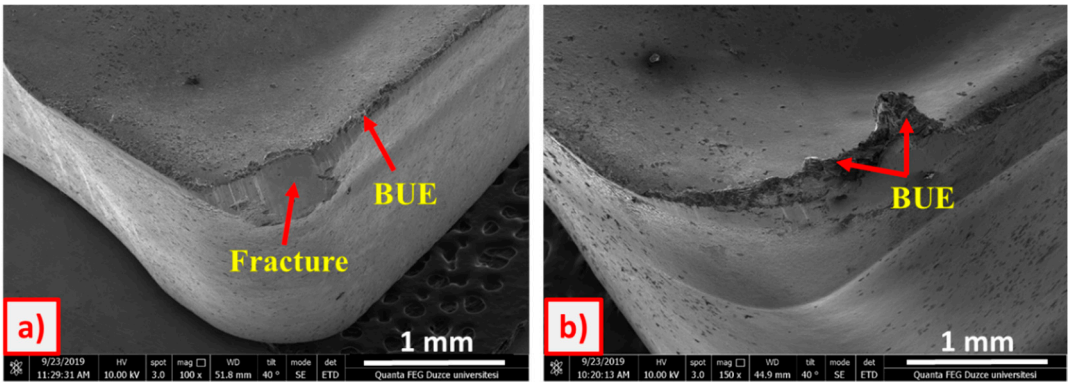

Figure 9. SEM images of tool wear that occur on cutting tools as a result of the milling of NiTi SMA (**a**) with the cutting tool with 0.4 mm r_ε, at high V_c (50 m/min) and f_z (0.14 mm/tooth) and (**b**) with the cutting tool with 0.8 mm r_ε, at low V_c (20 m/min) and f_z (0.03 mm/tooth).

The surface graph in Figure 10 shows the effect of the cutting parameters on the Vb values obtained as a result of this study. When the Vb obtained based on the f_z is examined, it is seen that the amount of heat generated in the environment increases as the f_z increases. Since NiTi SMAs have a low heat conduction coefficient, it has been observed that this heat cannot be removed from the environment and that the Vb on the tools increases with the effect of high heat and pressure [3,27]. The findings reveal that the cutting tool r_ε is an important factor in chip removal processes. The higher level of wear on the tool with small r_ε is attributed to the lower strength of the cutting tool, resulting from the cutting edge geometry. A larger r_ε forms a greater contact area on the cutting tool workpiece, which causes more friction of the cutting tool tip on the workpiece and an increase in the workpiece surface temperature. As a result, the workpiece material softens, while the cutting tools can maintain their hardness at high temperatures [27,30]. Cutting tools with large r_ε wear less and have a better tool life, which has been attributed to the high strength feature resulting from the cutting edge geometry [21].

The SEM and EDX analysis images of the tool wear that occurs during the milling process at 35 m/min V_c and 0.07 mm/tooth f_z are shown in Figure 11. When the figure is examined, it can be said that abrasive and adhesive wear mechanisms are effective on the BUE and fracture tool wear on the cutting tool. The image of the element analysis (EDX) made on fracture wear is shown in Figure 11d. When the results of the EDX analysis are examined, the adhesion of the workpiece material to the carbide base and the oxidation of W (Tungsten) in the carbide backing are observed. Fracture wear that occurs on cutting tools (Figure 11c) is caused by the weakening of the cutting edge strength and the increase in temperature and cutting strength [28,30].

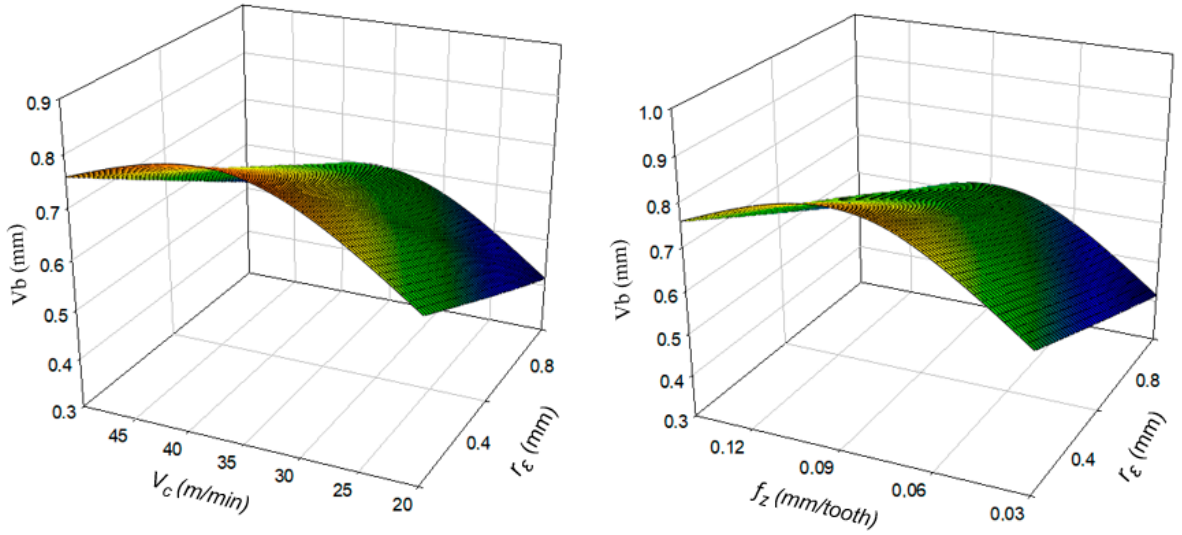

Figure 10. Effect of the cutting parameters on Vb.

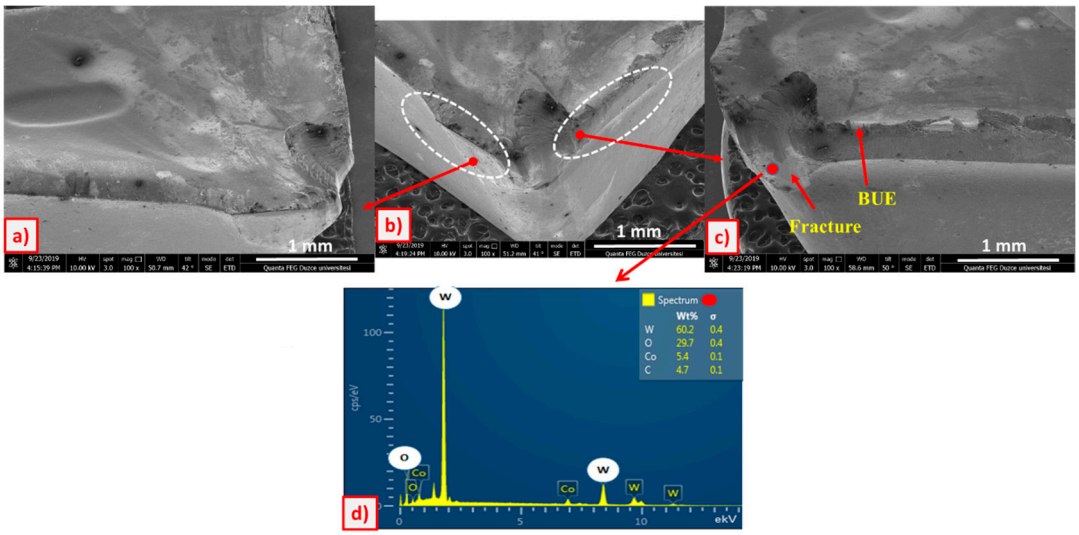

Figure 11. SEM images (**a**–**c**) and EDX analysis values (**d**) of tool wear that occur on cutting tools as a result of the milling of NiTi SMA with 0.4 mm r_ε under different machining parameters.

The SEM and EDX analysis images of tool wear that occurs during the milling process at 35 m/min V_c and 0.07 mm/tooth f_z are shown in Figure 12. As seen in the figure, the wear on the cutting tool is determined as Vb and BUE. It is thought that the reason for the Vb resulting from the abrasive wear mechanism is the hard carbide particles in the workpiece material [27]. BUE formation in the tool during the machining of NiTi SMA has been attributed to the low temperature between the tool-chip interface [28,30]. The image of the element analysis performed with EDX on BUE is shown in Figure 12d. When the EDX analysis results pertaining to the cutting tool are examined, it is determined that the carbide backing and the chips were exposed to oxidation.

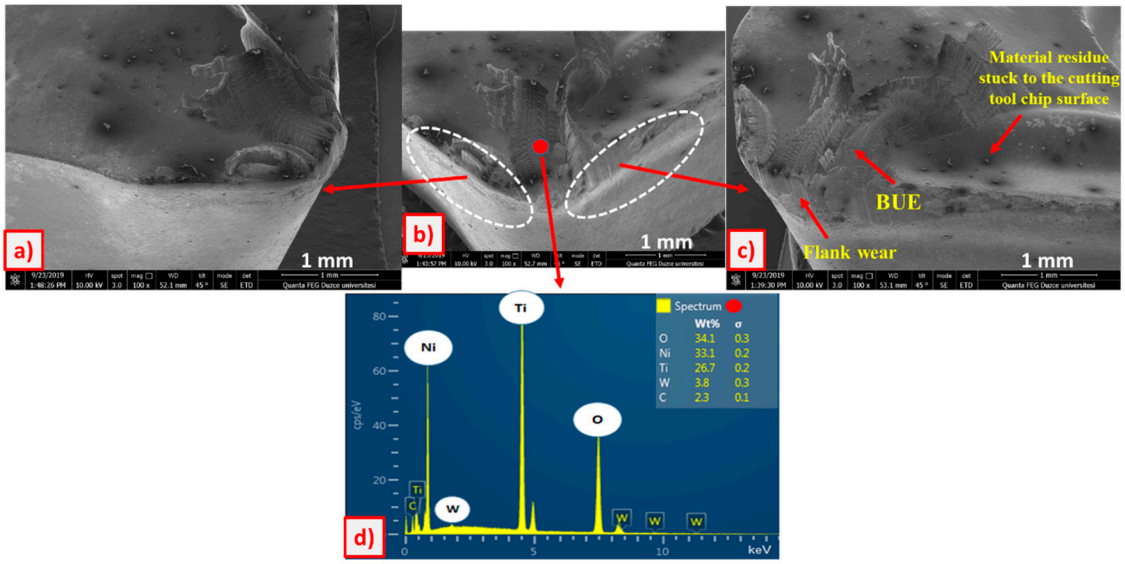

Figure 12. The SEM image (**a**–**c**) and EDX analysis values (**d**) of tool wear resulting from the milling of NiTi SMA with the cutting tool with 0.8 mm r_ε under different machining parameters.

3.4. Analysis of Variance (ANOVA) for Ra and Vb

After milling the NiTi SMA with carbide tools, analysis of variance (ANOVA) was applied to specify the impact of machining parameters on quality characteristics. ANOVA was conducted at 95% confidence level and 5% significance level. The optimum levels of the control factors with significant effects and the predicted optimum average surface roughness ($Ra_{\_opt}$) and flank wear ($Vb_{\_opt}$) with predicted optimum quality characteristics were determined from the ANOVA table.

The ANOVA values obtained for the Ra and Vb as a result of the experiment are shown in Table 8. As shown in the table, while the percentages of the contribution of the factors A, B and C to the Ra are 34.41%, 22.47% and 33.89%, respectively, the percentages of their contribution to Vb were found to be 27.10%, 12.51% and 50.62%, respectively. The results show that the factors that affect the Ra most are the cutting tool r_ε, f_z and V_c, respectively. On the other hand, the factors that affect Vb most are f_z, cutting tool r_ε and V_c, respectively.

Table 8. ANOVA results for average surface roughness (Ra) and flank wear (Vb).

	Variance Source	Degree of Freedom (df)	Sum of Squares (SS)	Mean Square (MS)	F	P	Contribution (%)
Average surface roughness (Ra)	A	1	0.0762	0.0762	44.68	0.000	34.41
	B	2	0.0498	0.0249	14.59	0.001	22.47
	C	2	0.0750	0.0375	22.00	0.000	33.89
	Error	12	0.0205	0.0017			9.24
	Total	17	0.2214				100
S = 0.04129 R^2 = 90.76% R^2 (adj) = 86.91%							
Flank wear (Vb)	A	1	0.2251	0.2251	33.27	0.000	27.10
	B	2	0.1039	0.0519	7.68	0.007	12.51
	C	2	0.4205	0.2102	31.07	0.000	50.62
	Error	12	0.0812	0.0068			9.77
	Total	17	0.8307				100
S =0.082257 R^2 = 90.23% R^2 (adj) = 86.15%							

3.5. Confirmation Experiments

In the Taguchi method, the confidence of optimization is confirmed experimentally after optimum results, and control factors and their levels are specified. With the optimization process, optimum surface roughness ($Ra_{\_opt}$) and optimum flank wear ($Vb_{\_opt}$) were determined. To specify the quality characteristic of validation experiments, the confidence interval (CI) was calculated. The CI predictive optimum quality characteristics for $Ra_{\_opt}$ and $Vb_{\_opt}$ were calculated using Equation (3) [20].

$$CI = \sqrt{F_{\alpha:1,V2} \cdot V_e \cdot \left(\frac{1}{n_{eff}} + \frac{1}{r}\right)} \quad (3)$$

In Equation (3), "$F_{\alpha:1,V2}$" is the F-ratio of the significant level α, "V2" is the degree of freedom of combined error variance, "r" is the number of repeated experiments, "Ve" is the combined error variance, and "n_{eff}" is the number of valid measurement tests. By using Equation (4). the number of valid measurement results "n_{eff}", is calculated [19,20].

$$n_{eff} = \frac{T_{exp}}{1 + dof} \quad (4)$$

In Equation (4), "T_{exp}" is the total number of experiments, and "dof" is the total degree of freedom of the factors used for estimation [20].

In the Taguchi method, the confidence of optimization is confirmed experimentally after reaching optimum results, and the levels are determined with control factors [19,20]. Using eighteen different experimental parameters, the $Ra_{\_opt}$ value obtained with real data was found to be 0.346 µm, while $Vb_{\_opt}$ value was found as 0.264 mm. The $Ra_{\_opt}$ value was calculated as 0.340 µm in the estimated combination of the Taguchi method. The estimated $Vb_{\_opt}$ value was calculated as 0.231 mm (Table 9).

Table 9. Comparison of the Ra and Vb.

		Average Surface Roughness		Flank Wear	
	Level	**Ra (µm)**	**S/N (dB)**	**Vb (mm)**	**S/N (dB)**
Random combination	$A_2B_3C_3$	0.585	4.657	0.796	1.982
Optimal combination (experiment)	$A_2B_1C_1$	0.346	9.218	0.264	11.568
Optimal combination (prediction)	$A_2B_1C_1$	0.340	8.917	0.231	11.205

The A2, B3, C3 combination randomly selected among 18 experiments conducted for Ra and Vb values, the optimum A2, B1, C1 combination, and the predicted A2, B1, C1 combination were compared (Table 9). According to the comparison, the Ra was reduced from 0.585 to 0.340 µm. The Vb was reduced from 0.796 mm to 0.231 mm. Since the estimated and experimental Ra and Vb values are very close to each other, it can be stated that the results obtained through the confirmation tests have shown the accuracy of the optimization with the use of the Taguchi method.

The $Ra_{\_opt}$ (0.340 µm) and $Vb_{\_opt}$ (0.231 mm) values estimated with the optimization process are given in Table 9. The confidence interval (CI) for Ra and Vb was calculated as specified in Equation (2) given in the previous section.

Based on the calculation in Equation (2), α = 0.05, $F_{\alpha:1,V2}$ = 4.747 (F ratio at 95% (in F table)), Ve_{Ra} = 0.0017 (from Table 8), Ve_{Vb} = 0.0068, r = 3, T_{exp} = 18, T_{dof} = 5 and n_{eff} = 3 were found. Using Equations (2) and (3), CI values were calculated as CI_{Ra} = ±0.073 and CI_{Vb} = ±0.147.

The CI value for estimated $Ra_{\_opt}$ and $Vb_{\_opt}$ at 95% confidence interval and 0.05 significance level is as follows:

$$[Ra_{\_opt} - CI_{Ra}] < Ra_{exp} < [Ra_{\_opt} + CI_{Ra}] \rightarrow [0.340 - 0.073] < 0.346 < [0.340 + 0.073] = 0.267 < 0.346 < 0.413$$

$$[Vb_{\_opt} - CI_{Vb}] < Vb_{exp} < [Vb_{\_opt} + CI_{Vb}] \rightarrow [0.231 - 0.147] < 0.264 < [0.231 + 0.147] = 0.084 < 0.264 < 0.378$$

The Ra_{exp} and Vb_{exp} values obtained from the experimental study remained within the CI. Therefore, by using the Taguchi method, the system optimization for Ra and Vb was achieved at 5% significance level.

4. Conclusions

In this study, which was carried out based on the findings of exhaustive research studies, the effect of the nose radius (r_ε) and cutting parameters (V_c and f_z) on the surface roughness (Ra) of NiTi shape memory alloy and tool wear in the milling process under dry cutting conditions was investigated. Optimum cutting conditions to machine NiTi alloy were determined so that they can be considered in future studies on coating applications on carbide cutting tools. It has been found that the cutting tool r_ε and f_z significantly affect Ra. The lowest Ra value (0.346 µm) was obtained with the cutting tools with 0.8 mm r_ε at 20 m/min V_c and 0.03 mm/tooth f_z. The lowest Vb was obtained with the cutting tools with 0.8 mm r_ε. According to the ANOVA results, while f_z is the most important variable affecting Vb, the cutting tool r_ε is the second most important variable. The types of tool wear observed on cutting tools used in cutting tests include Vb, BUE formation, mechanical fatigue fracture and cutting tool fracture wear. The basic wear mechanism was found to be abrasive and adhesive wear. When analyzed in terms of cutting parameters, it was determined that the increase in V_c and f_z generally increased the Vb of the cutting tool. Ra values increased with the increasing f_z. Increasing V_c improved Ra. In an optimization processes conducted using the Taguchi method for minimum Ra and minimum Vb, the results of the confirmation experiments were very close to predictive optimum values and remained within the tolerance limits of the confidence interval calculated for Ra and Vb.

Author Contributions: Performed and designed the experiments, E.A. and H.G.; verification experiments and wrote the paper, E.A., M.A.K., H.G., and D.O.; revised the paper and supervised the whole research, E.A., M.A.K., H.G., and D.O.; analyzed the data, E.A., M.A.K., H.G., and D.O. All authors have read and agreed to the published version of the manuscript.

Funding: This research received no external funding.

Acknowledgments: The experimental setup and the materials used in this study were designed within the scope of Karabuk University BAP Project No. FDK-2020-2197. The authors would like to thank Karabuk University, BAP Projects Unit due to their support.

Conflicts of Interest: The authors declare no conflict of interest.

References

1. Qader, İ.N.; Mediha, K.; Dagdelen, F.; Aydoğdu, Y. A review of smart materials: Researches and applications. *El-Cezeri J. Sci. Eng.* **2019**, *6*, 755–788.
2. Zhang, Y.; Xu, X. Transformation temperature predictions through computational intelligence for NiTi-based shape memory alloys. *Shape Mem. Superelasticity* **2020**, 1–13. [CrossRef]
3. Kaya, E.; Kaya, İ. Tool wear progression of PCD and PCBN cutting tools in high speed machining of NiTi shape memory alloy under various cutting speeds. *Diam. Relat. Mater.* **2020**, *105*, 107810. [CrossRef]
4. Otsuka, K.; Wayman, C. Mechanism of shape memory effect and superelasticity. In *Shape Memory Materials*; Cambridge University Press: Cambridge, UK, 1998; pp. 27–48.
5. Fu, C.H.; Liu, J.F.; Guo, Y.B.; Zhao, Q.Z. A Comparative Study on White Layer Properties by Laser Cutting vs. Electrical Discharge Machining of Nitinol Shape Memory Alloy. *Procedia CIRP* **2016**, *42*, 246–251. [CrossRef]

6. Daneshmand, S.; Monfared, V.; Lotfi Neyestanak, A.A. Effect of Tool Rotational and Al2O3 Powder in Electro Discharge Machining Characteristics of NiTi-60 Shape Memory Alloy. *Silicon* **2017**, *9*, 273–283. [CrossRef]
7. Lee, E.S.; Shin, T.H. An evaluation of the machinability of nitinol shape memory alloy by electrochemical polishing. *J. Mech. Sci. Technol.* **2011**, *25*, 963. [CrossRef]
8. Kong, M.C.; Srinivasu, D.; Axinte, D.; Voice, W.; McGourlay, J.; Hon, B. On geometrical accuracy and integrity of surfaces in multi-mode abrasive waterjet machining of NiTi shape memory alloys. *CIRP Ann.* **2013**, *62*, 555–558. [CrossRef]
9. Weinert, K.; Petzoldt, V. Machining of NiTi based shape memory alloys. *Mater. Sci. Eng. A* **2004**, *378*, 180–184. [CrossRef]
10. Kuppuswamy, R.; Yui, A. High-speed micromachining characteristics for the NiTi shape memory alloys. *Int. J. Adv. Manuf. Technol.* **2017**, *93*, 11–21. [CrossRef]
11. Weinert, K.; Petzoldt, V.; Kötter, D.; Buschka, M. Drilling of NiTi shape memory alloys. *Mater. Werkst.* **2004**, *35*, 338–341. [CrossRef]
12. Aslantaş, K.; Kaynak, Y. Micro milling of NiTi shape memory alloy and determination of critical chip thickness. *J. Fac. Eng. Archit. Gazi Univ.* **2018**, *2018*, 2–16.
13. Kaynak, Y.; Karaca, H.E.; Jawahir, I.S. Cutting Speed Dependent Microstructure and Transformation Behavior of NiTi Alloy in Dry and Cryogenic Machining. *J. Mater. Eng. Perform.* **2015**, *24*, 452–460. [CrossRef]
14. Wang, G.; Liu, Z.; Ai, X.; Huang, W.; Niu, J. Effect of cutting parameters on strain hardening of nickel–titanium shape memory alloy. *Smart Mater. Struct.* **2018**, *27*, 075027. [CrossRef]
15. Guo, Y.; Klink, A.; Fu, C.; Snyder, J. Machinability and surface integrity of Nitinol shape memory alloy. *CIRP Ann.* **2013**, *62*, 83–86. [CrossRef]
16. Skrócie, W. Industrial Applications of Shape Memory Alloys. Available online: https://www.totalmateria.com/page.aspx?ID=CheckArticle&site=ktn&LN=PL&NM=211 (accessed on 7 December 2020).
17. ISO 5608. *Turning and Copying Tool Holders and Cartridges for Indexable Inserts-Designation*; International Organization for Standardization (ISO): Geneva, Switzerland, 1995.
18. Gangele, A.; Mishra, A. Surface roughness optimization during machining of Niti shape memory alloy by EDM through Taguchi's technique. *Mater. Today Proc.* **2020**, *29*, 343–347. [CrossRef]
19. Karatas, M.A.; Gokkaya, H.; Nalbant, M. Optimization of machining parameters for abrasive water jet drilling of carbon fiber-reinforced polymer composite material using Taguchi method. *Aircr. Eng. Aerosp. Technol.* **2019**, *92*, 128–138. [CrossRef]
20. Karataş, M.A.; Motorcu, A.R.; Gökkaya, H. Optimization of machining parameters for kerf angle and roundness error in abrasive water jet drilling of CFRP composites with different fiber orientation angles. *J. Braz. Soc. Mech. Sci. Eng.* **2020**, *42*, 1–27.
21. Liang, X.; Liu, Z.; Wang, B. Multi-pattern failure modes and wear mechanisms of WC-Co tools in dry turning Ti–6Al–4V. *Ceram. Int.* **2020**, *46*, 24512–24525. [CrossRef]
22. Jadam, T.; Datta, S.; Masanta, M. Studies on chip morphology and modes of tool wear during machining of Ti-6Al-4V using uncoated carbide tool: Application of multi-walled carbon nanotubes added rice bran oil as nanocutting fluid. *Mach. Sci. Technol.* **2020**, 1–51. [CrossRef]
23. Rosnan, R.; Azmi, A.I.; Murad, M.N. Effects of Cutting Parameters on Tool Wear and Thrust Force in Drilling Nickel-Titanium (NiTi) Alloys Using Coated and Uncoated Carbide Tools. In *Key Engineering Materials*; Trans Tech Publications: Stafa-Zurich, Switzerland, 2018; pp. 111–115.
24. Kowalczyk, M. Cuting forces during precise turning of NiTi shape memory alloy. *Tech. Trans.* **2017**, *7*, 137–146.
25. Velmurugan, C.; Senthilkumar, V.; Dinesh, S.; Arulkirubakaran, D. Machining of NiTi-shape memory alloys-A review. *Mach. Sci. Technol.* **2018**, *22*, 355–401. [CrossRef]
26. Caliskan, H.; Altas, E. The effect of cutting conditions on cutting forces in milling of Ti6Al4V alloy. *Int. J. Eng. Technol. Nat. Sci.* **2015**, *13*, 13–22.
27. Caliskan, H.; Altas, E.; Panjan, P. Study of nanolayer AlTiN/TiN coating deposition on cemented carbide and its performance as a cutting tool. *J. Nano Res.* **2017**, *47*, 1–10. [CrossRef]
28. Mehta, K.; Gupta, K. Machining of Shape Memory Alloys. In *Fabrication and Processing of Shape Memory Alloys*; Springer: Berlin/Heidelberg, Germany, 2019; pp. 9–37.

29. Zailani, Z.A.; Mativenga, P.T. Effects of chilled air on machinability of NiTi shape memory alloy. *Procedia CIRP* **2016**, *45*, 207–210. [CrossRef]
30. Kaya, E.; Kaya, İ. A review on machining of NiTi shape memory alloys: The process and post process perspective. *Int. J. Adv. Manuf. Technol.* **2019**, *100*, 2045–2087. [CrossRef]